Measurement of molecular alignment with deep learning–based M–XFROG technique [Invited]

Wanchen Tao (陶皖辰)[1], Siqi Sun (孙思琦)[1], Lixin He (何立新)[1*], Yanqing He (何炎清)[1], Jianchang Hu (胡建昌)[1], Yu Deng (邓 宇)[1], Chengqing Xu (徐诚清)[1], Pengfei Lan (兰鹏飞)[1**], and Peixiang Lu (陆培祥)[1,2]

[1] Wuhan National Laboratory for Optoelectronics and School of Physics, Huazhong University of Science and Technology, Wuhan 430074, China
[2] Hubei Key Laboratory of Optical Information and Pattern Recognition, Wuhan Institute of Technology, Wuhan 430205, China

*Corresponding author: helx_hust@hust.edu.cn
**Corresponding author: pengfeilan@hust.edu.cn

We demonstrate a deep-learning neural network (DNN) method for the measurement of molecular alignment by using the molecular-alignment-based cross-correlation polarization-gating frequency resolved optical gating (M-XFROG) technique. Our network has the capacity for direct measurement of molecular alignment from the FROG traces. In a proof-of-principle experiment, we have demonstrated our method in O_2 molecules. With our method, the molecular alignment factor $\langle \cos^2 \theta \rangle (t)$ of O_2, impulsively excited by a pump pulse, was directly reconstructed. The accuracy and validity of the reconstruction have been verified by comparison with the simulations based on experimental parameters.

Keywords: molecular alignment; deep-learning neural network; M-XFROG.
DOI: 10.3788/COL202321.120021

1. Introduction

Molecular alignment using the interaction of molecules with femtosecond laser pulses plays a crucial role in the exploration of molecular reactions and dynamics. In the past two decades, significant progress has been made in achieving molecular alignment in various molecules[1–6]. This advancement has paved the way for widespread applications of molecular alignment in numerous scientific fields, such as multiphoton ionization[7,8], ultrashort pulse compression[9,10], molecular structure imaging[11–14], and high-order harmonic generation (HHG)[15–26]. Despite these achievements, attaining perfect molecular alignment in experimental settings remains a formidable challenge. In most cases, partial molecular alignment is obtained, resulting in measured results that represent an average over the distribution of molecular alignment. Consequently, an accurate measurement of the molecular alignment in the experiment is essential for probing the molecular dynamics and structure within the molecular frame.

Previously, it has been reported that molecular alignment can be indirectly determined using a comprehensive measurement of the molecular rotational temperature as well as the pump laser parameters including pulse duration, laser frequency, and pump intensity[27]. Since the molecular alignment is impulsively excited by a pump laser, the molecular rotational temperature determines the initial thermal distribution of the molecular rotational states, while the pump laser determines the redistribution of the rotational states after the laser-molecule interaction. With these parameters determined, molecular alignment then can be evaluated by numerical simulation of the time-dependent Schrödinger equation (TDSE) of the molecular rotational wavepacket[2]. To date, several methods have been reported to measure molecular rotational temperature in experiment, for instance, using the coherent anti-Stokes Raman scattering (CARS)[28–30] and degenerate four-wave mixing (DFWM)[31] processes and also using the Fourier spectrum of time-dependent HHG signals[32]. A simultaneous measurement of molecular rotational temperature and pump laser intensity is also demonstrated from the HHG signals[33–35] and the molecular alignment echo measurement[36]. However, these methods are still limited by their inherent restrictions. A direct and widely applicable method to measure the molecular alignment is still desired.

Analogous to the conventional frequency-resolved optical gating (FROG) technique, recently, a molecular-alignment-based cross-correlation polarization-gating frequency resolved optical gating (M-XFROG) technique was introduced to measure the ultrashort femtosecond lasers[37,38]. In M-XFROG, laser-induced impulsive molecular alignment serves as a transient gate function. The resulting FROG trace is given by[39,40]

$$I(\omega, \tau) = \left| \int_{-\infty}^{+\infty} E(t) G(t - \tau) \exp(-i\omega t) \mathrm{d}t \right|, \qquad (1)$$

where $E(t)$ is the electric field of the probe pulse, and $G(t) \propto |\langle \cos^2\theta \rangle(t) - 1/3|$ is the gate function, with $\langle \cos^2\theta \rangle(t)$ being the molecular alignment factor in experiment. A recovery algorithm, such as the principal component generalized projects algorithm (PCGPA), has routinely been used to retrieve the electric field of the probe pulse from the FROG trace[41]. In addition to the electric field of the probe pulse, the M-XFROG trace also encodes the information of molecular alignment, which therefore provides a potential way for measuring molecular alignment.

In this paper, we extend the M-XFROG technique to measure the molecular alignment by using a deep-learning neural network (DNN) method. Our network is trained to learn the relationship between the M-XFROG trace and the molecular alignment factor $\langle \cos^2\theta \rangle(t)$, which enables a direct measurement of the molecular alignment in experiment. We have demonstrated our scheme on a prototype O_2 molecule, both theoretically and experimentally. The accuracy and validity of our method have been examined by comparing the reconstructed molecular alignment factor $\langle \cos^2\theta \rangle(t)$ to the indirect measurement with the experimental parameters (including the molecular rotational temperature and the pump laser intensity) and also the retrieved electric field of the probe pulse to the PCGPA result.

2. Experiments and Methods

The network architecture used in this paper refers to a convolutional neural network named GoogLeNet[42], as shown in Fig. 1. Our network contains four convolutional layers, four Inception blocks, and three pooling layers. The convolutional layers enable the network to obtain enough information with fewer connection weight parameters. The output of the convolutional layer is calculated by multiplying the input by weight matrices called kernels and summing the product[43]. The kernels in each convolutional layer reduce the number of weights stored, which can optimize the accuracy and training time of the neural network. The Inception block is the key component of our network. Each block has four channels with kernels of different sizes (see inset in Fig. 1), which allows it to extract image information from multi-scale features. The pooling layers are used to reduce the size of the image, increase the computational speed, and improve the robustness of the extracted features.

Our network is trained on the simulated dataset. The input of the network is the M-XFROG trace which is simulated in terms of Eq. (1). In our simulations, the gate function $G(t)$ is obtained by solving the TDSE of the molecular rotational wavepacket with different molecular rotational temperatures and pump intensities (the wavelength and pulse duration can be measured from experiment)[44]. In our TDSE simulations, we adopt
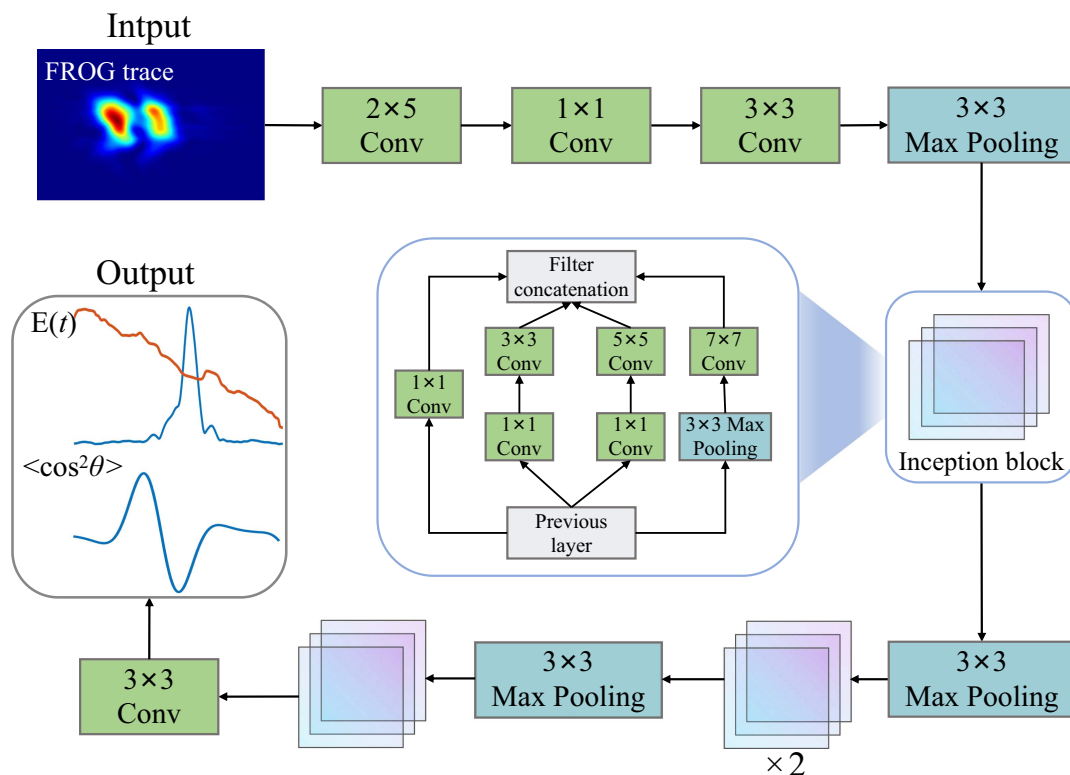

Fig. 1. Architecture of the neural network used for reconstructing the molecular alignment from the FROG trace. The inset shows the architecture of the Inception block.

oxygen (O_2) as the target molecule, as in our experiment (see below). For the electric field $E(t)$ of the probe pulse, we have measured its spectral intensity $A(\omega)$ in experiment. By generating a random spectral phase $\phi(\omega)$, we can get the electric field of the probe pulse in the frequency domain by $E(\omega)=\sqrt{A(\omega)}e^{i\phi(\omega)}$. Then, the time-domain $E(t)$ is obtained by the inverse Fourier transform of $E(\omega)$. In our training, we have created 80,000 data samples with different electric fields of the probe pulse and gate functions to construct the training set and test set. The network is trained using the GPU P100 on Kaggle to increase the training speed. In the process of training, the loss function is defined as the root mean squared error (RMSE) between the output and expectation. The training is stopped when the value of the loss function reaches the target set of 0.001.

We first demonstrate the validity and performance of our network by using the test dataset. Figure 2(a) shows a randomly selected M-XFROG trace as the input for the network. With the network, we can predict the outputs of the electric field of the probe pulse as well as the alignment factor $\langle\cos^2\theta\rangle(t)$ of the molecule. The predictions of our network are shown as the solid lines in Figs. 2(c) and 2(d). One can see that, the predicted electric field of the probe pulse, including both the laser intensity and phase, and also the alignment factor $\langle\cos^2\theta\rangle(t)$, agree well with the ground truth. With the predicted electric field and $\langle\cos^2\theta\rangle(t)$, we have recalculated the M-XFROG trace [see Fig. 2(b)], which is also in excellent agreement with the input in Fig. 2(a). These results prove the accuracy and validity of our network.

In the following, we demonstrate the application of our network to the experimental data. Figure 3 displays the schematic of the experimental setup. The experiment is carried out by using a commercial Ti:sapphire laser system (Astrella-USP-1K, Coherent), which delivers 35-fs, 800-nm laser pulses at a
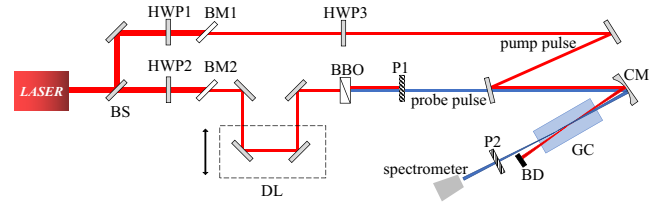

Fig. 3. Schematic diagram of the experimental setup. BS, beamsplitter; HWP, half-wave plate; BM, Brewster mirror; DL, delay line; BBO, BaB$_2$O$_4$; P, polarizer; BD, beam dump; GC, gas cell; CM, concave mirror.

repetition rate of 1 kHz. The output laser is split into two beams. One is used as a pump pulse to create molecular alignment. The other one is frequency doubled via a barium borate (BBO) crystal, serving as the probe pulse. The remaining 800-nm laser in the probe beam is filtered by a polarizer (P1), of which the transmission direction is perpendicular to the polarization of the 800-nm laser. A motorized delay line (DL) is installed in the arm of the probe pulse to adjust the time delay between these two pulses. The polarization of the pump pulse is rotated by 45° by using a half-wave plate (HWP) with respect to the probe pulse to ensure an optimal contrast ratio. These two pulses are focused into a gas cell filled with O_2 gas using a concave mirror ($f = 250$ mm) in the non-collinear geometry. The change in the polarization state of the probe pulse by the impulsive alignment of molecules was analyzed with another polarizer (P2) placed after the gas cell. The M-XFROG trace is then obtained by measuring the transmission spectra with a spectrometer at different time delays between the pump and probe pulses.

3. Results

Figure 4(a) shows the M-XFROG trace measured around the half rotational revival of O_2. By using the measured M-XFROG
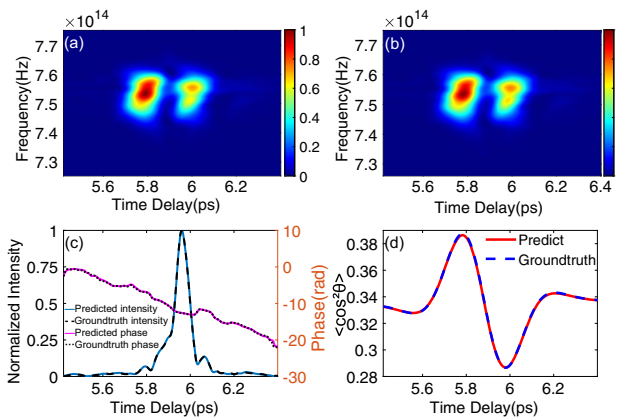

Fig. 2. (a) Simulated example of the M-XFROG trace. (b) M-XFROG trace constructed using the probe pulse and molecular alignment reconstructed by our network. (c) The reconstructed temporal intensity and phase of the probe pulse (solid lines). The dashed lines show the ground truth for comparision. (d) The reconstructed molecular alignment factor $\langle\cos^2\theta\rangle(t)$ (solid line). The dashed line shows the ground truth for comparision.
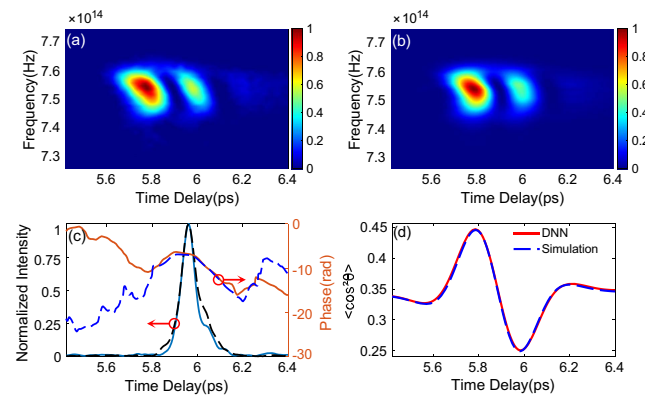

Fig. 4. (a) Measured M-XFROG trace around the half rotational revival of O_2. (b) The M-XFROG trace constructed using the probe pulse and the molecular alignment reconstructed by our network. (c) The reconstructed electric field of the probe pulse (solid lines). The dashed lines show the PCGPA results for comparison. (d) The reconstructed molecular alignment factor $\langle\cos^2\theta\rangle(t)$ (solid line) in experiment. The dashed line shows the simulation result based on the experimental parameters for comparison.
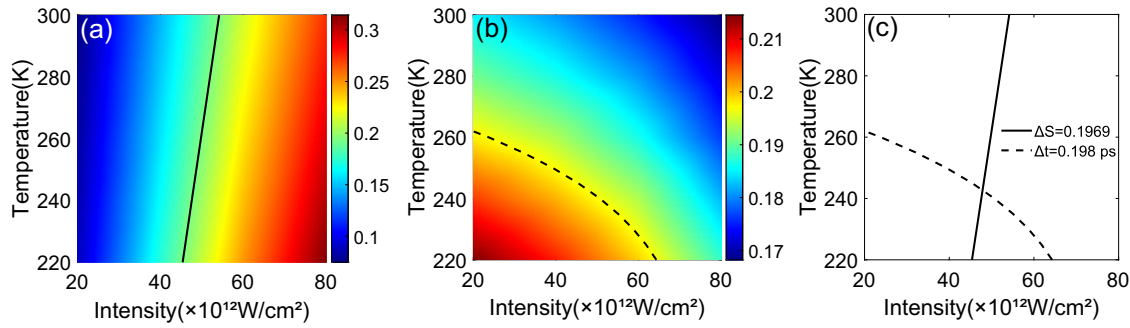
Fig. 5. (a) Modulation depth ΔS between the local extremas of the alignment factor as a function of the rotational temperature and pump intensity. The black solid line is a contour line for $\Delta S = 0.1969$. (b) Time interval Δt between the local extremas of the alignment factor as a function of the rotational temperature and pump intensity. The black dotted line is a contour line for $\Delta t = 0.198$ ps. (c) Contour lines for $\Delta S = 0.1969$ (solid line) and $\Delta t = 0.198$ ps (dotted line). The intersection indicates the molecular rotational temperature and the pump intensity.

trace as the input, we have predicted the electric field of the probe pulse and also the alignment factor $\langle \cos^2 \theta \rangle(t)$ in our experiment with our network. Corresponding results are shown as the solid lines in Figs. 4(c) and 4(d), respectively. With the predicted electric field of the probe pulse and also the alignment factor $\langle \cos^2 \theta \rangle(t)$, we have well reproduced the input (measured) M-XFROG trace [see Fig. 4(b)].

To evaluate the predictions, we have retrieved the laser field of the probe pulse with the commonly used PCGPA method. As shown in Fig. 4(c), the retrieved temporal intensity of the probe pulse (dashed lines) bascially agree with the reconstruction by our network. The temporal phase in the central part (5.8– 6.2 ps), where the laser intensity is predominant, is also in good agreement with our DNN reconstruction. Note that with PCGPA, the gate function $G(t)$, which is related to the molecular alignment in experiment, can be simultaneously extracted in the reconstruction. However, in this regard, to exactly determine the molecular alignment in experiment, some other parameters, such as the gas density and the interacting length between the gas and the pump laser, should be measured, which is still a challenging task in experiment. Here, we employ a method similar to that in Ref. [33] to assess the $\langle \cos^2 \theta \rangle(t)$ obtained with our network by simultaneously measuring the rotational temperature and pump laser intensity. As shown by the simulation results in Figs. 5(a) and 5(b), we find that the modulation depth ΔS, as well as the time interval Δt between the local extremas of the alignment factor $\langle \cos^2 \theta \rangle(t)$, depends sensitively on the molecular rotational temperature and the pump laser intensity. From the retrieved alignment factor $\langle \cos^2 \theta \rangle(t)$ (solid line) in Fig. 4(d), the ΔS and Δt are acquired to be 0.1969 and 0.198 ps, respectively. By comparing this to the simulation result in Fig. 5(a), we pick out all combinations of the rotational temperature and pump intensity that has $\Delta S = 0.1969$ [see the solid line in Fig. 5(a)]. Similarly, the result for $\Delta t = 0.198$ ps is also shown as the dotted line in Fig. 5(b). Putting these two contour lines together [see Fig. 5(c)], the intersection point of these two contour lines thus corresponds to the pending rotational temperature and pump intensity in our experiment, which are 242.66 K and 4.79×10^{13} W/cm², respectively. With these parameters, we can then determine the molecular alignment in our experiment

by solving the TDSE of molecular rotational wave functions. The calculated $\langle \cos^2 \theta \rangle(t)$ is shown as the dashed line in Fig. 4(d), which also agrees well with our network prediction.

4. Discussion

In summary, we have demonstrated a direct measurement of molecular alignment from the M-XFROG traces by using the deep-learning neural network (DNN). The network is trained on simulated data to learn the mapping relationship between the M-XFROG trace and the molecular alignment. With the trained network, the molecular alignment factor $\langle \cos^2 \theta \rangle(t)$, and the laser field of the probe pulse, are accurately reconstructed. The reconstructed alignment factor shows good agreement with the result indirectly obtained by measuring the molecular rotational temperature and pump laser intensity, proving the validity of our method. We have demonstrated our method using the O_2 molecule in experiment. In the future, the method proposed here can be extended to more complex molecules, e.g., asymmetric-top molecules and even to liquids.

Finally, it is worth mentioning that our method is based on the unique relationship between the M-XFROG trace and the molecular alignment factor $\langle \cos^2 \theta \rangle(t)$. In principle, it can also be applied to measure some other kinds of molecular alignment dynamics, such as adiabatic and permanent alignments, of which the degree is also described by $\langle \cos^2 \theta \rangle(t)$ [2,45–47]. However, in these cases, we may not employ the method in Fig. 5 to extract the experimental parameters, including the rotational temperature and the pump laser intensity from the curve of $\langle \cos^2 \theta \rangle(t)$, since the dependence of $\langle \cos^2 \theta \rangle(t)$ on these parameters may be different. Moreover, we observe that our method is not suitable for measuring the molecular orientation in experiment since the degree of molecular orientation is usually described by the factor $\langle \cos \theta \rangle(t)$ [48].

Acknowledgement

References

1. L. Cai, J. Marango, and B. Friedrich, "Time-dependent alignment and orientation of molecules in combined electrostatic and pulsed nonresonant laser fields," Phys. Rev. Lett. **86**, 775 (2001).
2. H. Stapelfeldt and T. Seideman, "Colloquium: aligning molecules with strong laser pulses," Rev. Mod. Phys. **75**, 543 (2003).
3. O. Ghafur, A. Rouzée, A. Gijsbertsen, W. K. Siu, S. Stolte, and M. J. J. Vrakking, "Impulsive orientation and alignment of quantum-state-selected NO molecules," Nat. Phys. **5**, 289 (2009).
4. Y. Ohshima and H. Hasegawa, "Coherent rotational excitation by intense nonresonant laser fields," Int. Rev. Phys. Chem. **29**, 619 (2010).
5. K. Lin, I. Tutunnikov, J. Qiang, J. Ma, Q. Song, Q. Ji, W. Zhang, H. Li, F. Sun, X. Gong, H. Li, P. Lu, H. Zeng, Y. Prior, I. Sh. Averbukh, and J. Wu, "All-optical field-free three-dimensional orientation of asymmetric-top molecules," Nat. Commun. **9**, 5134 (2018).
6. E. T. Karamatskos, S. Raabe, T. Mullins, A. Trabattoni, P. Stammer, G. Goldsztejn, R. R. Johansen, K. Długołecki, H. Stapelfeldt, M. J. J. Vrakking, S. Trippel, A. Rouzée, and J. Küpper, "Molecular movie of ultrafast coherent rotational dynamics of OCS," Nat. Commun. **10**, 3364 (2019).
7. I. V. Litvinyuk, K. F. Lee, P. W. Dooley, D. M. Rayner, D. M. Villeneuve, and P. B. Corkum, "Alignment-dependent strong field ionization of molecules," Phys. Rev. Lett. **90**, 233003 (2003).
8. T. K. Kjeldsen, C. Z. Bisgaard, L. B. Madsen, and H. Stapelfeldt, "Role of symmetry in strong-field ionization of molecules," Phys. Rev. A **68**, 063407 (2003).
9. J. Wu, H. Cai, H. Zeng, and A. Couairon, "Femtosecond filamentation and pulse compression in the wake of molecular alignment," Opt. Lett. **33**, 2593 (2008).
10. R. A. Bartels, T. C. Weinacht, N. Wagner, M. Baertschy, C. H. Greene, M. M. Murnane, and H. C. Kapteyn, "Phase modulation of ultrashort light pulses using molecular rotational wave packets," Phys. Rev. Lett. **88**, 013903 (2001).
11. J. Itatani, J. Levesque, D. Zeidler, H. Niikura, H. Pépin, J. C. Kieffer, P. B. Corkum, and D. M. Villeneuve, "Tomographic imaging of molecular orbitals," Nature **432**, 867 (2004).
12. C. Vozzi, M. Negro, F. Calegari, G. Sansone, M. Nisoli, S. De Silvestri, and S. Stagira, "Generalized molecular orbital tomography," Nat. Phys. **7**, 822 (2011).
13. C. Zhai, X. Zhang, X. Zhu, L. He, Y. Zhang, B. Wang, Q. Zhang, P. Lan, and P. Lu, "Single-shot molecular orbital tomography with orthogonal two-color fields," Opt. Express **26**, 2775 (2018).
14. L. He, X. Zhu, W. Cao, P. Lan, and P. Lu, "Attosecond spectroscopy for filming the ultrafast movies of atoms, molecules and solids," Chin. Phys. B **31**, 123301 (2022).
15. R. Velotta, N. Hay, M. B. Mason, M. Castillejo, and J. P. Marangos, "High-order harmonic generation in aligned molecules," Phys. Rev. Lett. **87**, 183901 (2001).
16. J. Itatani, D. Zeidler, J. Levesque, M. Spanner, D. M. Villeneuve, and P. B. Corkum, "Controlling high harmonic generation with molecular wave packets," Phys. Rev. Lett. **94**, 123902 (2005).
17. T. Kanai, S. Minemoto, and H. Sakai, "Ellipticity dependence of high-order harmonic generation from aligned molecules," Phys. Rev. Lett. **98**, 053002 (2007).
18. O. Smirnova, Y. Mairesse, S. Patchkovskii, N. Dudovich, D. Villeneuve, P. Corkum, and M. Y. Ivanov, "High harmonic interferometry of multi-electron dynamics in molecules," Nature **460**, 972 (2009).
19. L. He, P. Lan, A. T. Le, B. Wang, B. Wang, X. Zhu, P. Lu, and C. D. Lin, "Real-time observation of molecular spinning with angular high-harmonic spectroscopy," Phys. Rev. Lett. **121**, 163201 (2018).
20. P. M. Kraus, B. Mignolet, D. Baykusheva, A. Rupenyan, L. Horný, E. F. Penka, G. Grassi, O. I. Tolstikhin, J. Schneider, F. Jensen, L. B. Madsen, A. D. Bandrauk, F. Remacle, and H. J. Wörner, "Measurement and laser control of attosecond charge migration in ionized iodoacetylene," Science **350**, 790 (2015).
21. L. He, S. Sun, P. Lan, Y. He, B. Wang, P. Wang, X. Zhu, L. Li, W. Cao, P. Lu, and C. D. Lin, "Filming movies of attosecond charge migration in single molecules with high harmonic spectroscopy," Nat. Commun. **13**, 4595 (2022).
22. A. Rupenyan, J. B. Bertrand, D. M. Villeneuve, and H. J. Wörner, "All-optical measurement of high-harmonic amplitudes and phases in aligned molecules," Phys. Rev. Lett. **108**, 033903 (2012).
23. Y. He, L. He, P. Lan, B. Wang, L. Li, X. Zhu, W. Cao, and P. Lu, "Direct imaging of molecular rotation with high-order-harmonic generation," Phys. Rev. A **99**, 053419 (2019).
24. B. Wang, L. He, Y. He, Y. Zhang, R. Shao, P. Lan, and P. Lu, "All-optical measurement of high-order fractional molecular echoes by high-order harmonic generation," Opt. Express **27**, 30172 (2019).
25. Y. Huang, J. Zhao, Z. Shu, Y. Zhu, J. Liu, W. Dong, X. Wang, Z. Lü, D. Zhang, J. Yuan, J. Chen, and Z. Zhao, "Ultrafast hole deformation revealed by molecular attosecond interferometry," Ultrafast Sci. **2021**, 9837107 (2021).
26. Y. Chen, X. Zhu, P. Lan, and P. Lu, "Background-free detection of molecular chirality using a single-color beam [Invited]," Chin. Opt. Lett **20**, 100004 (2022).
27. E. Péronne, M. D. Poulsen, C. Z. Bisgaard, H. Stapelfeldt, and T. Seideman, "Nonadiabatic alignment of asymmetric top molecules: field-free alignment of iodobenzene," Phys. Rev. Lett. **91**, 043003 (2003).
28. P. Huber-Wälchli, D. M. Guthals, and J. W. Nibler, "Cars spectra of supersonic molecular beams," Chem. Phys. Lett. **67**, 233 (1979).
29. M. D. Duncan, P. Österlin, and R. L. Byer, "Pulsed supersonic molecular-beam coherent anti-Stokes Raman spectroscopy of C_2H_2," Opt. Lett. **6**, 90 (1981).
30. T. Lang, M. Motzkus, H. M. Frey, and P. Beaud, "High resolution femtosecond coherent anti-Stokes Raman scattering: determination of rotational constants, molecular anharmonicity, collisional line shifts, and temperature," J. Chem. Phys. **115**, 5418 (2001).
31. T. Hornung, H. Skenderović, K.-L. Kompa, and M. Motzkus, "Prospect of temperature determination using degenerate four-wave mixing with sub-20 fs pulses," J. Raman Spectrosc. **35**, 934 (2004).
32. K. Yoshii, G. Miyaji, and K. Miyazaki, "Measurement of molecular rotational temperature in a supersonic gas jet with high-order harmonic generation," Opt. Lett. **34**, 1651 (2009).
33. Y. He, L. He, P. Wang, B. Wang, S. Sun, R. Liu, B. Wang, P. Lan, and P. Lu, "Measuring the rotational temperature and pump intensity in molecular alignment experiments via high harmonic generation," Opt. Express **28**, 21182 (2020).
34. X. Guo, C. Jin, Z. He, J. Yao, X.-X. Zhou, and Y. Cheng, "Retrieval of molecular alignment and identification of multiple-orbital contribution by using polarized high harmonics from aligned N_2 molecules," Opt. Express **29**, 1613 (2021).
35. C. Jiang, H. Jiang, Y. Chen, B. Li, C. D. Lin, and C. Jin, "Genetic-algorithm retrieval of the molecular alignment distribution with high-order harmonics generated from transiently aligned CO_2 molecules," Phys. Rev. A **105**, 023111 (2022).
36. P. Wang, L. He, Y. He, J. Hu, S. Sun, P. Lan, and P. Lu, "Rotational echo spectroscopy for accurate measurement of molecular alignment," Opt. Lett. **47**, 1033 (2022).
37. P. Lu, J. Liu, H. Li, H. Pan, J. Wu, and H. Zeng, "Cross-correlation frequency-resolved optical gating by molecular alignment for ultraviolet femtosecond pulse measurement," Appl. Phys. Lett. **97**, 061101 (2010).
38. J. Liu, Y. Feng, H. Li, P. Lu, H. Pan, J. Wu, and H. Zeng, "Supercontinuum pulse measurement by molecular alignment based cross-correlation frequency resolved optical gating," Opt. Express **19**, 40 (2011).
39. R. Trebino, K. W. DeLong, D. N. Fittinghoff, J. N. Sweetser, M. A. Krumbügel, B. A. Richman, and D. J. Kane, "Measuring ultrashort laser pulses in the time-frequency domain using frequency-resolved optical gating," Rev. Sci. Instrum. **68**, 3277 (1997).
40. D. J. Kane and R. Trebino, "Single-shot measurement of the intensity and phase of an arbitrary ultrashort pulse by using frequency-resolved optical gating," Opt. Lett. **18**, 823 (1993).
41. D. J. Kane, "Real-time measurement of ultrashort laser pulses using principal component generalized projections," IEEE J. Sel. Top. Quantum Electron. **4**, 278 (1998).

42. C. Szegedy, W. Liu, Y. Jia, P. Sermanet, S. Reed, D. Anguelov, D. Erhan, V. Vanhoucke, and A. Rabinovich, "Going deeper with convolutions," in *IEEE Conference on Computer Vision and Pattern Recognition (CVPR)* (2015), p. 1.

43. J. White and Z. Chang, "Attosecond streaking phase retrieval with neural network," Opt. Express **27**, 4799 (2019).

44. T. Szidarovszky, M. Jono, and K. Yamanouchi, "LIMAO: cross-platform software for simulating laser-induced alignment and orientation dynamics of linear-, symmetric- and asymmetric tops," Comput. Phys. Commun. **228**, 219 (2018).

45. T. Seideman, "Rotational excitation and molecular alignment in intense laser fields," J. Chem. Phys. **103**, 7887 (1995).

46. T. Seideman, "On the dynamics of rotationally broad, spatially aligned wave packets," J. Chem. Phys. **115**, 5965 (2001).

47. Md. Z. Hoque, M. Lapert, E. Hertz, F. Billard, D. Sugny, B. Lavorel, and O. Faucher, "Observation of laser-induced field-free permanent planar alignment of molecules," Phys. Rev. A **84**, 013409 (2011).

48. H. Li, W. Li, Y. Feng, H. Pan, and H. Zeng, "Field-free molecular orientation by femtosecond dual-color and single-cycle THz fields," Phys. Rev. A **88**, 013424 (2013).